



Determination of starch crystallinity with the Fourier-transform terahertz spectrometer

Nakajima, Shusaku
Horiuchi, Shuhei
Ikehata, Akifumi
Ogawa, Yuichi

(Citation)

Carbohydrate Polymers, 262:117928

(Issue Date)

2021-06-15

(Resource Type)

journal article

(Version)

Accepted Manuscript

(Rights)

© 2021.

This manuscript version is made available under the CC-BY-NC-ND 4.0 license
<http://creativecommons.org/licenses/by-nc-nd/4.0/>

(URL)

<https://hdl.handle.net/20.500.14094/90008257>



1 Title

2 Determination of starch crystallinity with the Fourier-transform terahertz spectrometer

3

4 Authors

5 Shusaku Nakajima^{a,b,✉}, Shuhei Horiuchi^c, Akifumi Ikehata^b, Yuichi Ogawa^{c,✉}

6

7 ^aAffiliation: Graduate School of Agricultural Science, Kobe University, 1-1 Rokkodai-
8 cho, Nada, Kobe 657-8501, Japan

9 ^bAffiliation: Food Research Institute, National Agriculture and Food Research
10 Organization, 2-1-12 Kannondai, Tsukuba 305-8642, Japan

11 ^cAffiliation: Graduate School of Agriculture, Kyoto University, Kitashirakawa-
12 Oiwakecho, Sakyo-ku, Kyoto 606-8502, Japan

13 [✉]Corresponding authors

14 E-mail: shu.nakajima@shark.kobe-u.ac.jp (S. Nakajima)

15 E-mail: ogawayu@kais.kyoto-u.ac.jp (Y. Ogawa)

16

17

18

Abstract

We measured the terahertz (THz) spectra of native, amorphous, and dried starches derived from corn and potato using the Fourier-transform (FT) system and compared these spectra to the X-ray diffraction (XRD) patterns. Both native corn and potato starches had seven absorption peaks in the terahertz regions, but five peaks were observed in the amorphous states. While spectral changes slightly occurred in corn starch even after drying, increase and decrease in the terahertz peak intensities were obtained in potato starch during drying. Similar changes in both starches during amorphization and drying were obtained in the X-ray diffraction patterns, and the correlations were found between terahertz peaks and the X-ray signals. Since the intensity of the peak at 9.0 THz was correlated with crystallinity obtained using an X-ray diffraction ($r^2=0.98$), our data indicate that the Fourier-transform terahertz spectrometer can be a new analytical device to measure the starch crystallinity.

Keywords

Starch, Crystallinity, Terahertz spectroscopy, X-ray diffraction

1. Introduction

Starch consisting of monomeric glucose is the predominant form of carbohydrate reserve found in diverse agricultural products, such as cereals, tubers, beans, and fruits. Starch consists of two glucans, namely amylose and amylopectin. Amylose is a primarily linear structure connected by α (1 \rightarrow 4) glycosidic linkages and is generally thought to be in an amorphous state. Amylopectin demonstrates a semi-crystalline state and a highly branched structure connected by α (1 \rightarrow 4) and α (1 \rightarrow 6) glycosidic linkages. In amylopectin, the crystalline region is formed by parallel double helices and an amorphous area at the branching point of the cluster chains (Blazek & Gilbert, 2011; Pérez & Bertoft, 2010). The crystalline structures of starch granules are affected by the amylose-amylopectin ratio, degree of branching, and chain length of the amylopectin.

The degree of crystallinity, defined as the percentage of crystalline regions within the total material, is one of the factors for determining starch function and utilization. In the process of enzymatic hydrolysis of starch in humans, the crystalline regions in the starch granule provide barriers to the diffusion and adsorption of the hydrolyzed enzymes, resulting in a slow digestion rate. However, starch with low crystallinity is rapidly digested due to the higher accessibility of enzymes (Blazek & Gilbert, 2010; Zhang, Dhital, & Gidley, 2013). Thus, a correlation was found between crystallinity and the

digestion rate of starch (Bao, Li, Wu, & Ouyang, 2018; Carrera, Utrilla-Coello, Bello-Pérez, Alvarez-Ramirez, & Vernon-Carter, 2015; Zhang et al., 2014). The crystalline structure of starch is also important in industrial fields. For instance, the amylose-amylopectin ratio and crystalline structure determine the strength and stiffness of starch plastics (van Soest & Vliegenthart, 1997). The network structure is formed by connecting starches with plasticizers during starch plastic production, but the short length of the amylopectin chain weakens the materials. Starch properties are also involved in bioethanol production (Yangcheng, Jiang, Blanco, & Jane, 2013). Unlike starch with a high content of amylopectin with long chains and high crystallinity, starch with a high content of amylose or amylopectin with short chains and low crystallinity contributed to enhanced starch hydrolysis and yield of bioethanol.

X-ray diffraction (XRD) has been the major method used for determining the crystalline structures in starch at the molecular level (long-range order) and has been used to measure the crystallinity of starch. The crystallinity of carbohydrate polymers can be calculated in three methods, peak height, peak deconvolution, and amorphous subtraction (Park, Baker, Himmel, Parilla, & Johnson, 2010). The amorphous subtraction method has been commonly used for starch measurement (Lopez-Rubio, Flanagan, Gilbert, & Gidley, 2008; Nara & Komiya, 1983). According to the XRD patterns, native starch granules have

15%–45% crystallinity and can be classified into three types depending on their botanical sources (Zobel, 1988). A-type diffraction patterns are present in cereals, and B-type diffraction patterns are present in the roots and tubers. Bean and specific fruit starches show C-type diffraction, which is the combination of the A- and B-types. The main difference between the A- and B-type starches is the structure between the double helices and water molecules within the crystalline lattice (Imberty, Chanzy, Perez, Buléon, & Tran, 1988a; Imberty & Perez, 1988b; Popov et al., 2009). A-type starch has a monoclinic structural unit, characterized by the tightly compacted helices with fewer water molecules. B-type starch has a hexagonal structural unit with ample space between the helices for the accumulation of numerous water molecules. The water molecules among the double helices are connected to a starch chain or other water molecules via a hydrogen bond.

Spectroscopy is one of the useful analytical methods for exploring the molecular structure and interaction between the surrounding molecules or solvents. Conventional vibrational spectroscopies (near- and mid-infrared) have been used to determine starch structure in the short-range order (atomic level) (Kizil, Irudayaraj, & Seetharaman 2002; van Soest, Tournois, de Wit, & Vliegenthart, 1995). However, these spectroscopic techniques are not sensitive to starch crystallinity in the long-range order (Pozo et al., 2018; Sevenou, Hill, Farhat, & Mitchell, 2002; Warren, Gidley, & Flanagan, 2016)

because the apparent vibrational modes of the functional groups and structures in the short-range order are reflected in the near- and mid-infrared spectra. Nuclear magnetic resonance (NMR) spectroscopy is also used to analyze starch structures in short-range order because of the different chemical shift patterns of ordered and non-ordered portions. Although previous studies have found a correlation between NMR data and starch crystallinity (Flanagan, Gidley, & Warren, 2015), NMR cannot directly access the starch structure in long-range order. Thus, direct measurement of starch crystallinity has not been achieved using conventional spectroscopies.

Terahertz (THz) or far-infrared waves are generally referred to as the frequency range from 100 GHz to 30 THz ($3.3\text{--}1000\text{ cm}^{-1}$) and recent advances in optical devices have made it possible to use THz spectroscopy to explore new applications (Tonouchi, 2007). In THz spectra, we can obtain information about the intermolecular and the lattice vibrational modes dominated by the polymorphs (King, Buchanan, & Korter, 2011; True, Schroeck, French, & Schmuttenmaer, 2011). For example, crystallized molecules have shown absorption bands attributed to the hydrogen bond networks, the *van der Waals* forces, and framework vibrations, while no such bands have been observed in the amorphous state due to the lack of crystalline structures in the long-range order (Otsuka, Nishizawa, Fukura, & Sasaki, 2012; Strachan et al., 2004; Walther, Fischer, & Jepsen,

2003). Previous studies have also found correlations between the THz spectra and the crystallinity of polymers (Azeyanagi & Ohki, 2018), carbohydrates (Takeuchi et al., 2012; Vieira & Pasquini, 2014), and pharmaceutical materials (da Silva, Vieira, Rohwedder, Pasquini, & Pereira, 2017; Strachan et al., 2005) obtained by XRD. For instance, Vieira and Pasquini (2014) estimated the crystallinity of cellulose using THz spectra in the range of 0.7–3.4 THz ($23.3\text{--}113\text{ cm}^{-1}$) with partial least squares (PLS) regression analysis. da Silva et al. (2017) used THz spectra from 0.4 to 4.4 THz ($13.3\text{--}147\text{ cm}^{-1}$) to determine the crystallinity of mebendazole. Compared to the near- and mid-infrared spectra (da Silva, Gonçalves, Vasconcelos, Fernanda Pimentel, & Pereira, 2015), THz spectroscopy provided a higher determination coefficient and fewer errors in estimating the crystallinity of mebendazole. The authors remarked on the advantage of using THz spectroscopy to directly access information about the crystalline structure, compared to the use of near- and mid-infrared spectroscopy.

THz spectroscopy is commonly performed using the time-domain system (TDS) and Fourier transform (FT) system. The former provides the phase directly and is suitable for evaluating the optical properties in the THz region, but an expensive femtosecond pulse laser system is indispensable. The latter is a system that shifts the conventional mid-infrared spectrometer to the low-frequency side, and its principle is same as that of FT

infrared spectroscopy. While the TDS provides THz spectra in the lower frequencies below 5.0 THz (167 cm^{-1}), the broadband spectra in the higher frequency regions can be obtained by the FT system. Since the region observed by the FT system is the boundary between intramolecular vibration and intermolecular vibration, researchers of far-infrared spectroscopy have long been interested (Han et al., 2001). Although most researchers have employed the TDS (Azeyanagi & Ohki, 2018; da Silva et al., 2017; Strachan et al., 2005; Takeuchi et al., 2012; Vieira & Pasquini, 2014), which is commercially obtained, starch has not demonstrated any distinctive absorption peaks in the lower frequencies measured by this system (Jiang, Ge, Lian, Zhang, & Xia, 2016). However, our study used the FT system and identified inherent peaks in starch (Nakajima, Shiraga, Suzuki, Kondo, & Ogawa, 2019). Therefore, we hypothesized that these starch peaks may be an index for the starch structure in the long-range order and FT-THz spectrometer may have the potential to be a new analytical method for elucidation of the crystallinity estimation.

The FT-THz spectrometer also has advantages for crystalline measurements, compared to conventional XRD. The price of the THz device is lower than that of the X-ray diffractometer. Moreover, unlike X-rays with ionizing properties, THz waves have much lower energies; hence, THz spectroscopy can monitor starch structures without causing ionization and damage to the structure.

Thus, in this study, we aimed to examine whether FT-THz spectrometer could be a new analytical method for determining starch crystallinity. We measured the THz spectra of corn (A-type) and potato (B-type) starches with different crystallinity and compared them with the XRD patterns. Based on the obtained THz and XRD data, the model for crystallinity estimation was developed. Herein, we present possible causes for the spectral differences between the A- and the B-types with respect to the long-range starch structures.

2. Materials and methods

2.1. Chemicals

We purchased standard corn and potato starches from Wako Pure Chemical Industries, Ltd. Polyethylene powder with a particle size $8\pm1\ \mu\text{m}$ was used to dilute samples for the THz measurement. Native starches were used as the crystalline starches. To obtain stable spectral data, fine particles were required, thus all starch samples were passed through a $32\ \mu\text{m}$ mesh sieve before measurement.

2.2. Preparation of amorphous starches

Amorphous starches were prepared according to a method described in a report (Kim, Kim, & Shin, 1997) with some modifications. Starches were suspended in distilled water (10%, w/v) and heated at $95\ ^\circ\text{C}$ for complete gelatinization. The gelatinized starches were

163 mixed with 99% ethanol (starch gel : ethanol = 1 : 4, v/v), thoroughly stirred, and the
164 mixed solvent was removed. The residuals were dried at 40 °C overnight until they
165 achieved a constant weight. The samples were ground into powder with a mortar and
166 pestle, and passed through a 32 µm mesh sieve.

167 2.3. *Drying process*

168 We used a drying process to modify the starch crystallinity. While drying has slight or
169 little influence on the crystallinity of the A-type starches, dynamic structural changes in
170 the long-range order have been reported in the B-type starches (Gunaratne & Hoover,
171 2002; Jacobs & Delcour, 1998). Thus, corn starch (A-type) was dried in an air oven at
172 120 °C for 960 min only, while potato starch (B-type) was dried at the same temperature
173 for 5 min, 10 min, 30 min, 120 min, and 960 min. After cooling, the starches were passed
174 through a 32 µm mesh sieve.

175 2.4. *THz measurement*

176 Starches were mixed with polyethylene powder at 5% mass concentration (sample: 8
177 mg; polyethylene: 152 mg). The mixtures were pressed at 15 kN for 10 min into solid
178 pellets with a 13 mm diameter and 1.25±0.05 mm thickness. The absorbance of the pellet
179 was then measured using an originally remodeled FT spectrometer (FARIS-1s, JASCO
180 Co.) with a ceramic light source from 3.0 THz to 13.5 THz (100–450 cm⁻¹) at a resolution

of 0.12 THz (4 cm^{-1}) according to a method in our previous measurement (Nakajima et al., 2019). To enhance the signal to noise (SN) ratio, 300 scans were recorded and averaged. Measurement time was approximately 5 min. After replacing a pellet, the same measurement was repeated further twice to evaluate three different points for each pellet, and the average value was used. The spectrum of pure polyethylene (152 mg) was also recorded as a reference spectrum. Additionally, we measured the absorbance of three individual pellets for each condition and averaged the absorbance spectra. As an incoherent light source was used in the FT system, we could avoid an etalon peak, which is clearly observed in TDS equipped with a coherence laser. The peak position in the THz regions was determined from the second derivative spectra. Since the particle size and pellet thickness were adjusted, the baseline spectra were stable and other spectral processes, such as normalization, were not required.

2.5. XRD analysis

XRD patterns were measured using a diffractometer (Smart Lab, Rigaku Co.). Data were obtained over the 2θ range of 4° – 40° at 0.05° interval with a scan speed of 3° min^{-1} , using Cu-K α radiation with $\lambda = 1.541\text{ \AA}$. The “d” spacings were calculated according to the Bragg’s law. After baseline correction and the Savitzky-Golay smoothing, the relative crystallinity of samples was calculated according to the *Hermans* method reported by

Nara and Kamiya (1983). Briefly, the upper crystalline part was separated with a smooth curve connecting each point of minimum intensity of the crystalline peaks and the lower part was defined as an amorphous area, using Matlab software (See Fig. S1). Starch crystallinity was calculated by crystalline area / (crystalline + amorphous) area.

3. Results and discussion

3.1. Crystalline and amorphous starches

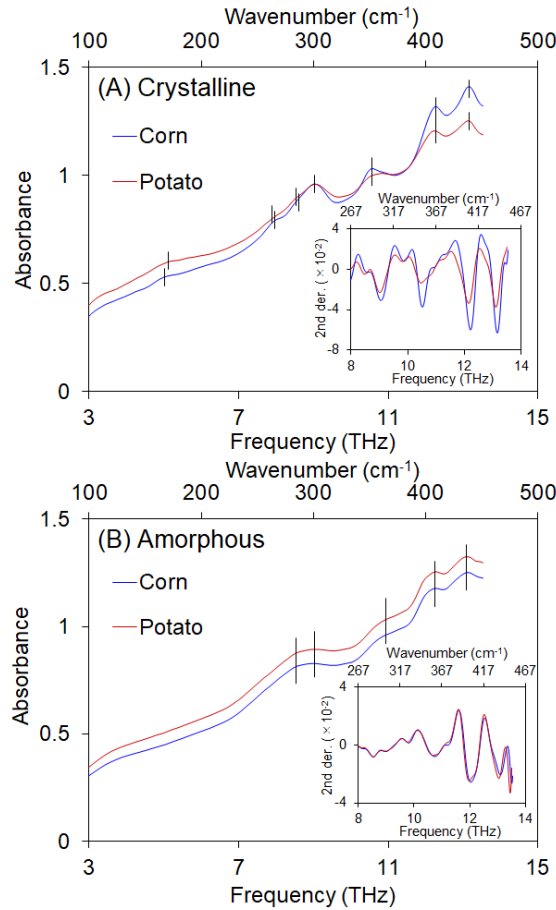
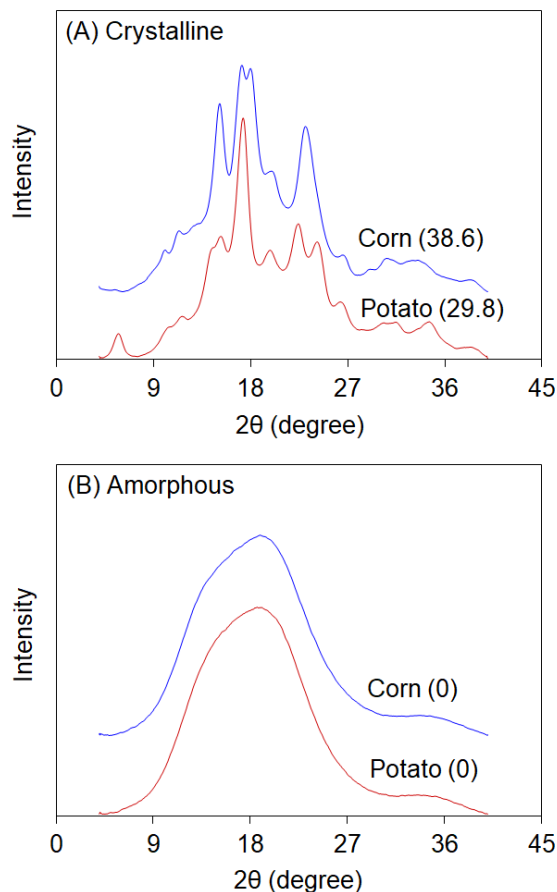


Fig. 1. Absorbance spectra of (A) crystalline (native) and (B) amorphous starches. Vertical lines indicate absorption peaks, and insets represent the second derivative spectra

209 in the range of 8.0 THz–13.5 THz (267 cm^{-1} – 450 cm^{-1}).

210



212 **Fig. 2.** XRD patterns of (A) crystalline and (B) amorphous starches. The values in
213 parenthesis indicate crystallinity.

214

215 We first compared the THz spectra of corn and potato starches with crystalline and
216 amorphous states (Fig. 1). Corn starch had four main peaks at 9.0 THz (300 cm^{-1}), 10.5
217 THz (350 cm^{-1}), 12.2 THz (407 cm^{-1}), and 13.2 THz (440 cm^{-1}), and three shoulder peaks
218 at 4.9 THz (163 cm^{-1}), 7.9 THz (263 cm^{-1}) and 8.6 THz (287 cm^{-1}). Potato starch exhibited

similar peaks at 5.1 THz (170 cm^{-1}), 7.8 THz (260 cm^{-1} , albeit very weak), 8.5 THz (283 cm^{-1}), 9.0 THz, 10.5 THz, 12.2 THz and 13.1 THz (437 cm^{-1}), but intensities of the four main peaks were lower than those of corn starch (see inset in Fig. 1A). Additionally, potato starch had higher absorbance in the lower frequencies. The causes for higher peak intensities of corn starch and higher absorbance of potato starch in the lower frequencies have been discussed later.

Compared to the crystalline starches, no clear spectral difference was acquired between corn and potato starches after amorphization (Fig. 1B). While the absorption peaks around 5.0 THz (167 cm^{-1}) and 8.0 THz (267 cm^{-1}) observed in the crystalline states were hardly visible, amorphous starches had two overlapping peaks at 8.5 THz and 9.0 THz, and three peaks at 10.7 THz (357 cm^{-1}), 12.0 THz (400 cm^{-1}), and 13.1 THz. Although four peaks at 9.0 THz, 10.7 THz, 12.0 THz and 13.1 THz became less intense after amorphization, the peak intensity at 8.5 THz was stronger (second derivative signals of native corn, native potato, amorphous corn, and amorphous potato were 3.1×10^{-3} , 4.8×10^{-3} , 7.8×10^{-3} and 8.0×10^{-3} , respectively), suggesting that the peak was sensitive to the amorphous structure of starch. Noteworthy, we observed the different peak frequencies, except for peaks at 9.0 THz, 10.5 THz, and 12.2 THz, between native corn and potato starches, and peak shifts after amorphization. These spectral features may originate from differences in the starch

structure, because structural differences have been strongly reflected at peak positions in the THz regions (King et al., 2011; Otsuka et al., 2012; Strachan et al., 2004; True et al., 2011; Walther et al., 2003). However, in this study, it is difficult to elucidate the cause for peak positions and shifts without a more detailed analysis.

Fig. 2 shows the XRD patterns of crystalline and amorphous starches. Crystalline corn starch displayed the A-type diffraction, having clear peaks at $2\theta = 15^\circ$, 17° , 18° , and 23° . Potato starch displayed the B-type diffraction, having clear peaks at $2\theta = 5.5^\circ$, 17° , 22° , and 24° . Crystallinity in native corn and potato starches was 38.6% and 29.8%, respectively. However, amorphous corn and potato starches exhibited no distinctive diffraction peaks and crystalline structures. We defined the crystallinity in amorphous starches to be 0%. The crystallinity of crystalline starches was slightly higher than previously reported (dos Santos, Leonel, Garcia, do Carmo, & Franco, 2016; Pozo et al., 2018). Compared to large particles, fine starch particles contribute to higher crystallinity because the content of amorphous amylose decreases in fine particles (Ao & Jane, 2007; Wang, Tang, Fu, Huang, & Zhang, 2016). For these reasons, the higher crystallinity observed in this study could be due to fine starch particles.

3.2. *Dried starches*

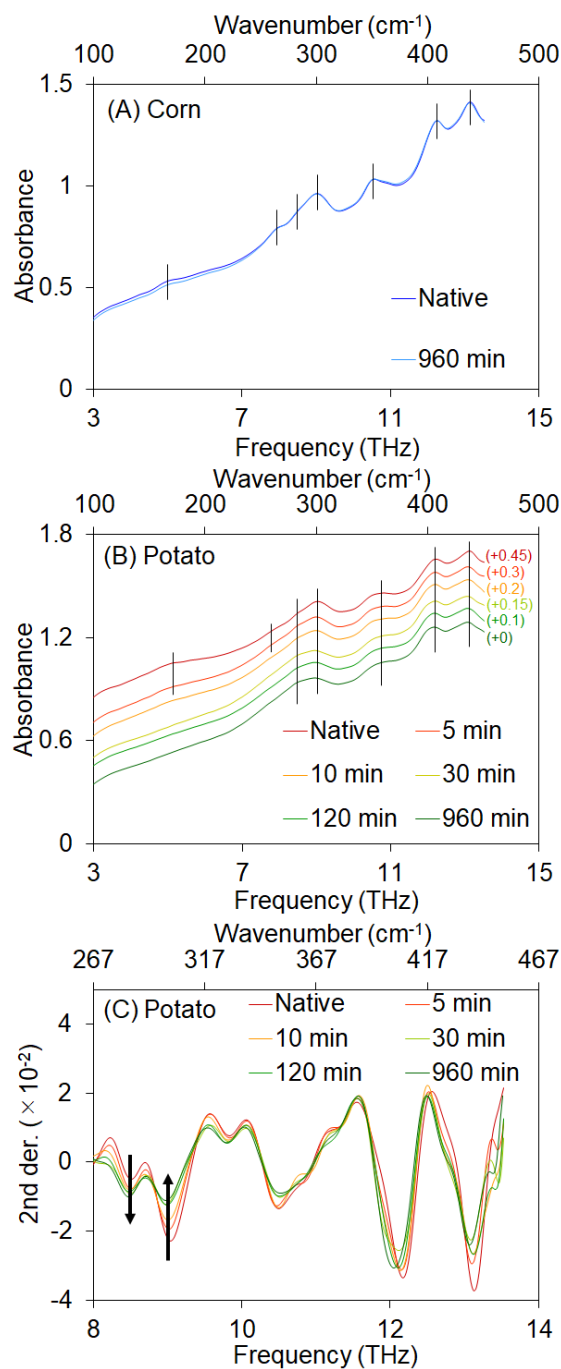


Fig. 3. Absorbance spectra of dried (A) corn and (B) potato starches. The absorbance spectra of potato starch were offset vertically for clear spectral features, +0.1–0.45. Vertical lines indicate the absorption peaks. (C) Second derivative spectra of the dried potato starch in the range of 8.0 THz–13.5 THz (267 cm^{-1} – 450 cm^{-1}). Black arrows mark

the two peaks showing the continuous changes during drying.

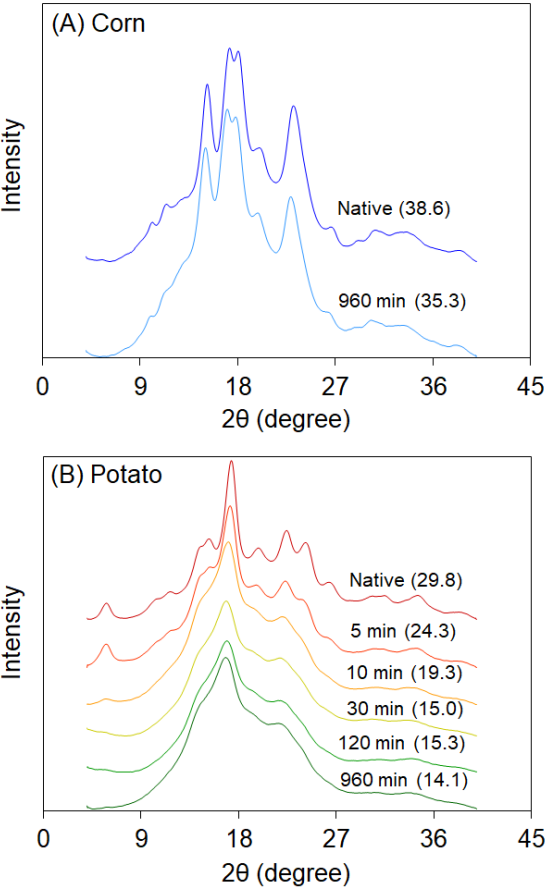


Fig. 4. XRD patterns of dried (A) corn and (B) potato starches. The values in parenthesis indicate crystallinity.

The THz spectra of corn starch indicated slight changes even after 960 min of drying (Fig. 3A), while distinct spectral changes occurred in the potato starch during drying (Fig. 3B, 3C). The two peaks at 5.1 THz and 7.8 THz disappeared within the first 10 min, and intensities of the other five peaks were also altered during drying. Notably, the continuous

increase and decrease in peak intensities were found at 8.5 THz and 9.0 THz.

Similar changes were measured in the XRD patterns of dried starches. The four clear peaks were slightly shifted to lower angles, and crystallinity decreased by 3.3% in the dried corn starch, compared to that in the native corn (Fig. 4A). In contrast, the progressive collapse of the crystalline structure and decline in the crystallinity were observed in potato starch during drying (Fig. 4B). The clear and small peaks became weaker or disappeared during the first 10 min, and two clear peaks at $2\theta = 17^\circ$ and 22° were observed after 30 min. The crystallinity of potato starch decreased by 15.7% after 960 min of drying.

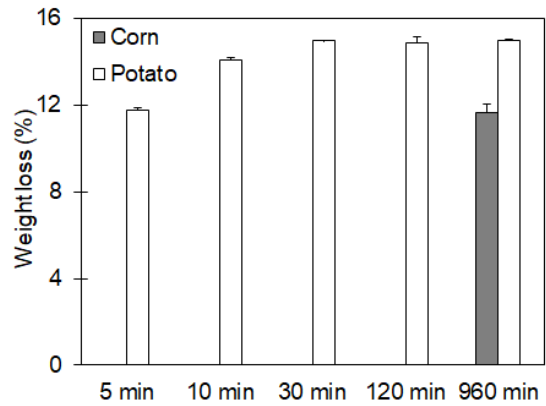


Fig. 5. Weight loss in corn and potato starches during drying (n=3).

The weight loss attributed to the evaporation of water during drying is shown in Fig. 5. The weight loss in corn and potato starches after 960 min of drying was 11.7% and 15.0%, respectively. Notably, the weight loss was constant in potato starch after 30 min, thus

potato starch lost water molecules during the first 30 min. These results indicate that water molecules have little influence on the crystalline structure of corn starch. Additionally, the decrease in crystallinity of potato starch during the first 30 min of drying could mainly be due to water loss or water-starch interaction, while that after 30 min could be due to the collapse of the starch structure. Previous XRD measurements have reported similar data in the A- and the B-type starches during drying, and the B-type starches enriched with water molecules were more easily altered than the A-type starches (Gunaratne & Hoover, 2002; Jacobs & Delcour, 1998).

3.3. THz-XRD correlation

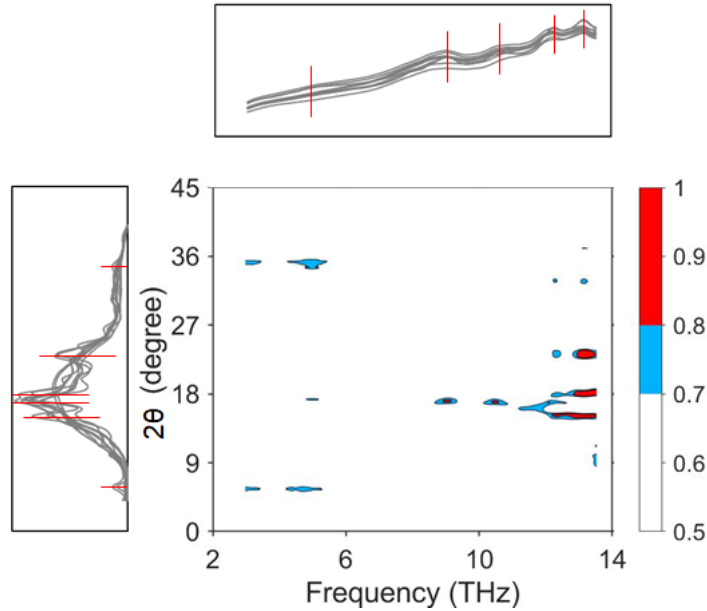


Fig. 6. Heat map of the correlation coefficient between the THz spectra and the XRD patterns. Red lines indicate the THz and XRD peaks having correlation.

297

298 Statistical heterospectroscopy is a method to investigate the correlation between
299 different kinds of spectroscopic data acquired on multiple samples (Crockford et al.,
300 2006). Since the THz spectra, especially peak intensities, and the XRD patterns exhibited
301 similar behavior during amorphization and drying, we used this analytical method to the
302 THz spectra and the XRD patterns in order to further elaborate the starch spectra.

303 In Fig. 6 we present the correlation coefficient between the THz spectra and the XRD
304 patterns of the ten starch samples; the cells with low ($0.7 < r \leq 0.8$) and high ($0.8 < r$)
305 positive values are marked in blue and red, respectively. No negative correlation was
306 found. The five THz peaks showed correlations with the XRD patterns. The shoulder peak
307 around 5.0 THz had low correlations with $2\theta = 5.5^\circ$, 17° , and 35° , and these results were
308 consistent with the decrease or disappearance of THz and XRD peaks during the first 10
309 min of drying (Fig. 4B). High correlations were obtained between the four main peaks.
310 The peaks at 9.0 THz and 10.5 THz correlated with $2\theta = 17^\circ$, and 12.2 THz with $2\theta = 15^\circ$.
311 Additionally, the peak around 13.0 THz was correlated with $2\theta = 15^\circ$, 18° and 23° . We
312 further explored the THz peaks having high correlations with the XRD patterns. Since 2θ
313 = 15° – 23° correspond to 3.94 Å–5.96 Å of “d” spacing base on the Bragg’s law, our data
314 suggests that the four peaks above 9.0 THz may be assigned to the vibrational modes of

these distances in the crystalline lattice.

3.4. THz spectral features and starch structure

Carbohydrates, including starch, have been found to exhibit non-covalent modes (hydrogen-bond networks and inter-crystalline forces) and covalent modes (skeletal deformations such as -C-C-C- and -C-O-C-) of interaction in the THz regions (Cael, Koenig, & Blackwell, 1975; Hineno, 1977; Yang, Weng, Ferraro, & Wu, 2001; Zhibankov, Andrianov, & Marchewka, 1997). Hineno (1977) investigated the peak assignments of sugar in the THz regions based on the observed spectra and calculated the one-molecular model. The observed peak positions correlated with the calculated vibrational frequencies in the region above 7.5 THz (250 cm^{-1}), though calculations based on the model did not explain all the observed spectra because of intermolecular interactions in the region below 7.5 THz. Thus, the frequency boundary of the non-covalent and covalent modes located around 7.5 THz, and the THz spectra obtained in our study contained information on both vibrational modes of starch.

In starch granules, double helices are stabilized by non-covalent hydrogen bonds and *van der Waals* forces, which are weaker than covalent forces (Lan et al., 2016; Xu et al., 2019). During gelatinization and amorphization, weak non-covalent bonds are destroyed, and starch granules lose their crystalline structure. The disappearance of two peaks around

5.0 THz and 8.0 THz in amorphous starches suggests that these two peaks in native starch granules may be attributed to non-covalent forces connecting the helix structure. The other five peaks observed above 8.5 THz, however, continued to exist after amorphization and disordered the crystalline structures; thus, exhibition of these peaks could be attributed to the covalent modes of starch. The double helix structure and vibrational modes are illustrated in the graphical abstract.

The heat map (Fig. 6) further supports the assignments of four peaks observed above 9.0 THz. In double helices, six monomeric glucose molecules have one turn of the helix, showing 21.0 Å along the helix axis (Imberty, Buléon, Tran, & Perez, 1991; Sarko & Wu, 1978; Zobel, 1988). Thus, the spacing of 3.94 Å–5.96 Å, as shown in Fig. 6, corresponded to a distance of approximately 1.5 glucose molecules. This spacing was markedly longer than the vibrational modes of the functional groups (C-O, C-H, and O-H) in the near- and mid-infrared regions. Additionally, the distance spanning a hydrogen-bonded pair of glucose units within a double helix was 2.5 Å–3.0 Å and that of the non-covalent force connecting double helices was at least 11.0 Å (the distance between the two double helices) (Imberty et al., 1988a; Imberty & Perez, 1988b). Magnitude of non-covalent forces in starch granules was smaller or greater than the obtained spacing of 3.94 Å–5.96 Å. These starch structures suggest that the interaction between the glucose monomers (i.e.,

covalent force) may be consistent with the obtained distance. We also examined the correlation coefficient between non-covalent regions below 8.0 THz and covalent regions above 8.0 THz. Although THz peaks around 5.0 THz and 10.5 THz had low correlation, no high THz-THz correlation was found (see Fig. S2). These results indicate that the covalent and non-covalent modes in starch granule are not synchronized.

The A- and B-type starches have the structural differences between the double helices and water molecules within the crystalline lattice, as described in the Introduction (Sarko & Wu, 1978; Imberty et al., 1988a; Imberty & Perez, 1988b). Since the numerous water molecules in the B-type starch are connected to a starch chain or other water molecules via a hydrogen bond, dehydration during drying influences the crystalline structures and XRD patterns in the B-type starches (Kainuma & French, 1972; Nara, Mori, & Komiya, 1978). Drying induced evaporation of water molecules from starch granules and movement of double helices into the ample space originally occupied by the evaporated water, resulting in the collapse of the crystalline structure (Gunaratne & Hoover, 2002). A similar disruption of the crystalline structure in potato starch was observed in our study (Fig. 4B).

The water molecules and hydrogen bond network among the helices in the B-type starch may also be responsible for higher absorbance of potato starch in the lower

369 frequencies, as shown in Fig. 1A. Corn and potato starches exposed to 960 min of drying
370 showed similar absorbance spectra in the lower frequencies (see Fig. S3). Thus, water
371 molecules may be attributed as the cause of higher absorbance of potato starch, but the
372 THz spectra of starches cannot be easily interpreted. The weight loss attributed to water
373 evaporation in corn and potato starches during drying was 11.7% and 15.0%, respectively,
374 as shown in Fig. 5. If water molecules are directly reflected on the absorbance spectra in
375 the lower frequencies, the decline in absorbance should theoretically occur in both
376 starches, but this was not observed for corn starch (Fig. 3A). Although the numerous
377 water molecules among the helices are only observed in the B-type starch as described
378 above, both the A- and B-type starches have bulk and bound water (Tang, Godward, &
379 Hills, 2000), which have relatively less influence on the crystalline structure. If the THz
380 spectra in the lower frequency regions are sensitive to the vibrational modes of water
381 molecules among the helices (or interactions between the water and starch), it is
382 reasonable that a decrease in absorbance after drying would be observed only in potato
383 starch. Additionally, the evaporation of bulk and bound water could cause weight loss in
384 both corn and potato starches. Thus, we hypothesize that the absorbance of water among
385 the helices may be apparent in the THz spectra, resulting in a higher absorbance of potato
386 starch (B-type) in the lower frequency regions.

3.5. Estimation of crystallinity

Table 1. The linear regression models for starch crystallinity using six peaks (n=10).

Peak (THz)	4.9 and 5.1	8.5 and 8.6	9.0	10.5	12.2	13.1 and 13.2
r^2	0.76	0.58	0.98	0.69	0.69	0.74
RMSE (%)	4.1	6.2	1.1	4.9	4.8	4.3

Previous THz studies have used linear least squares regression using a single peak (Azeyanagi & Ohki, 2018; Takeuchi et al., 2012) or PLS regression using multi-spectra for crystallinity estimation (da Silva et al., 2017; Strachan et al., 2005; Vieira & Pasquini, 2014). Since starch had absorption peaks, we used linear regression analysis in this study. Table 1 shows the model performance to estimate starch crystallinity by six different peaks at and around 5.0 THz, 8.5 THz, 9.0 THz, 10.5 THz, 12.2 THz, and 13.0 THz. The details of these models are shown in Fig. S4. These models were obtained from second derivative signals of the six peaks via comparison with the objective crystallinity values calculated by the XRD ranged from 0% to 38.6% for ten different samples (corn starch crystallinity: 38.6%, 35.3%, and 0%; potato starch crystallinity: 29.8%, 24.3%, 19.3%, 15.3%, 15.0%, 14.1%, and 0%). To correct baseline fluctuations in absorbance spectra, we used the dip intensity in the second derivative spectra based on methods described by a previous study (Nakajima et al., 2019). The best model was generated by using the peak

at 9.0 THz, having r^2 of 0.98 and root mean squared error (RMSE) of 1.1%. Thus, this peak was found to be sensitive to structural changes in the long-range order and a useful index for crystallinity estimation, as hypothesized. Although the peak at 8.5 THz exhibited continuous changes during drying, this peak resulted in the lowest r^2 among the five peaks. This result was consistent with the statistical heterospectroscopy showing no correlation between peak at 8.5 THz and the XRD patterns, as shown in Fig. 6. Since the main four peaks above 9.0 THz were correlated with crystallinity ($r^2=0.69-0.98$), crystallinity influenced these peak intensities. Thus, the reason for higher peak intensities above 9.0 THz in corn starch (Fig. 1A, inset), compared to potato starch, could be a higher crystallinity.

Since measurement of starch crystallinity is an important aspect in various fields, previous studies have investigated new analytical methods, including spectroscopy (Pozo et al., 2018; Sevenou et al., 2002; Warren et al., 2016), instead of XRD. However, infrared spectroscopy and THz-TDS were not useful as an alternative method for the reasons described in Introduction. In contrast, we found that the starch peak at 9.0 THz determined by the FT system could be a valuable index for crystallinity estimation. The most important finding of this study is that, in the case of starch, the peak important for crystallinity measurement appears in the frequency covered by the FT system, but not by

TDS.

4. Conclusions

In this study, we found synchronized data between the THz spectra and the XRD patterns of starches, and the useful THz peak attributed covalent vibrational modes for crystallinity estimation. In XRD analysis, the extraction and purification pretreatments are required to measure starch crystallinity in agricultural products due to the influences of other plant matrices. We already found that the starch peak at 9.0 THz did not overlap with the constituent saccharides (Nakajima et al., 2019). In addition, the THz spectra of dry food samples enriched with starch provided this peak, which was attributed to starch and was not affected by other plant matrices. These results suggest that THz spectroscopy may measure starch crystallinity in food samples without pretreatments. To refine this method, further studies of THz measurements in food samples and crystallinity estimation will be required.

Declaration of Competing Interest

The authors report no declarations of interest.

Acknowledgments

The authors thanks Kyoto University Nano Technology Hub in “Nanotechnology Platform Project” sponsored by the Ministry of Education, Culture, Sports, Science and Technology (MEXT), Japan for using the X-ray diffractometer. This research was supported by grants from the Project of the NARO Bio-oriented Technology Research Advancement Institution (Research program on development of innovative technology).

References

- Ao, Z., & Jane, J. (2007). Characterization and modeling of the A- and B-granule starches of wheat, triticale, and barley. *Carbohydrate Polymers*, 67, 46–55.
- Azeyanagi, C., & Ohki, Y. (2018). Terahertz spectroscopic estimation of crystallinity of poly (phenylene sulfide). *Journal of Applied Polymer Science*, 135, 1–10.
- Bao, W., Li, Q., Wu, Y., & Ouyang, J. (2018). Insights into the crystallinity and in vitro digestibility of chestnut starch during thermal processing. *Food Chemistry*, 269, 244–251.
- Blazek, J., & Gilbert, E. P. (2010). Effect of enzymatic hydrolysis on native starch granule structure. *Biomacromolecules*, 11, 3275–3289.
- Blazek, J., & Gilbert, E. P. (2011). Application of small-angle X-ray and neutron

458 scattering techniques to the characterisation of starch structure: A review.
 459 *Carbohydrate Polymers*, 85, 281–293.

460 Cael, J. J., Koenig, J. L., & Blackwell, J. (1975). Infrared and Raman spectroscopy of
 461 carbohydrates. Part VI: Normal coordinate analysis of V-amylose. *Biopolymers*, 14,
 462 1885–1903.

463 Carrera, Y., Utrilla-Coello, R., Bello-Pérez, A., Alvarez-Ramirez, J., & Vernon-Carter,
 464 E. J. (2015). In vitro digestibility, crystallinity, rheological, thermal, particle size and
 465 morphological characteristics of pinole, a traditional energy food obtained from
 466 toasted ground maize. *Carbohydrate Polymers*, 123, 246–255.

467 Crockford, D. J., Holmes, E., Lindon, J. C., Plumb, R. S., Zirah, S., Bruce, S. J., ...
 468 Nicholson, J. K. (2006). Statistical heterospectroscopy, an approach to the integrated
 469 analysis of NMR and UPLC-MS data sets: Application in metabonomic toxicology
 470 studies. *Analytical Chemistry*, 78, 363–371.

471 da Silva, V. H., Gonçalves, J. L., Vasconcelos, F. V. C., Fernanda Pimentel, M., & Pereira,
 472 C. F. (2015). Quantitative analysis of mebendazole polymorphs in pharmaceutical
 473 raw materials using near-infrared spectroscopy. *Journal of Pharmaceutical and*
 474 *Biomedical Analysis*, 115, 587–593.

475 da Silva, V. H., Vieira, F. S., Rohwedder, J. J. R., Pasquini, C., & Pereira, C. F. (2017).

476 Multivariate quantification of mebendazole polymorphs by terahertz time domain
 477 spectroscopy (THZ-TDS). *Analyst*, 142, 1519–1524.

478 dos Santos, T. P. R., Leonel, M., Garcia, É. L., do Carmo, E. L., & Franco, C. M. L.
 479 (2016). Crystallinity, thermal and pasting properties of starches from different potato
 480 cultivars grown in Brazil. *International Journal of Biological Macromolecules*, 82,
 481 144–149.

482 Flanagan, B. M., Gidley, M. J., & Warren, F. J. (2015). Rapid quantification of starch
 483 molecular order through multivariate modelling of ¹³C CP/MAS NMR spectra.
 484 *Chemical Communications*, 51, 14856–14858.

485 Gunaratne, A., & Hoover, R. (2002). Effect of heat-moisture treatment on the structure
 486 and physicochemical properties of tuber and root starches. *Carbohydrate Polymers*,
 487 49, 425–437.

488 Han, P. Y., Tani, M., Usami, M., Kono, S., Kersting, R., & Zhang, X. C. (2001). A direct
 489 comparison between terahertz time-domain spectroscopy and far-infrared Fourier
 490 transform spectroscopy. *Journal of Applied Physics*, 89, 2357–2359.

491 Hineno, M. (1977). Infrared spectra and normal vibration of β-d-glucopyranose.
 492 *Carbohydrate Research*, 56, 219–227.

493 Imberty, A., Chanzy, H., Perez, S., Buléon, A., & Tran, V. (1988a). The double-helical

494 nature of the crystalline part of A-starch. *Journal of Molecular Biology*, 20, 365–378.

495 Imberty, A., & Perez, S. (1988b). A revisit to the three-dimensional structure of B-type

496 starch. *Biopolymers*, 27, 1205–1221.

497 Imberty, A., Buléon, A., Tran, V., & Perez, S. (1991). Recent advances in knowledge of

498 starch structure. *Starch/Stärke*, 43, 375–384.

499 Jacobs, H., & Delcour, J. A. (1998). Hydrothermal modifications of granular starch, with

500 retention of the granular structure: A Review. *Journal of Agricultural and Food*

501 *Chemistry*, 46, 2895–2905.

502 Jiang, Y., Ge, H., Lian, F., Zhang, Y., & Xia, S. (2016). Early detection of germinated

503 wheat grains using terahertz image and chemometrics. *Scientific Reports*, 6, 1–9.

504 Kainuma, K., & French, D. (1972). Naegeli amyloextrin and its relationship to starch

505 granule structure. II. Role of water in crystallization of B-starch. *Biopolymers*, 11,

506 2241–2250.

507 Kim, J. O., Kim, W. S., & Shin, M. S. (1997). A comparative study on retrogradation of

508 rice starch gels by DSC, X-Ray and α -Amylase methods. *Starch/Stärke*, 49, 71–75.

509 King, M. D., Buchanan, W. D., & Korter, T. M. (2011). Identification and quantification

510 of polymorphism in the pharmaceutical compound diclofenac acid by terahertz

511 spectroscopy and solid-state density functional theory. *Analytical Chemistry*, 83,

512 3786–3792.

513 Kizil, R., Irudayaraj, J., & Seetharaman, K. (2002). Characterization of irradiated starches
 514 by using FT-Raman and FTIR Spectroscopy. *Journal of Agricultural and Food*
 515 *Chemistry*, 50, 3912–3918.

516 Lan, X., Xie, S., Wu, J., Xie, F., Liu, X., & Wang, Z. (2016). Thermal and enzymatic
 517 degradation induced ultrastructure changes in canna starch: Further insights into
 518 short-range and long-range structural orders. *Food Hydrocolloids*, 58, 335–342.

519 Lopez-Rubio, A., Flanagan, B. M., Gilbert, E. P., & Gidley, M. J. (2008). A novel
 520 approach for calculating starch crystallinity and its correlation with double helix
 521 content: A combined XRD and NMR study. *Biopolymers*, 89, 761–768.

522 Nakajima, S., Shiraga, K., Suzuki, T., Kondo, N., & Ogawa, Y. (2019). Quantification of
 523 starch content in germinating mung bean seedlings by terahertz spectroscopy. *Food*
 524 *Chemistry*, 294, 203–208.

525 Nara, S., Mori, A., & Komiya, T. (1978). Study on relative crystallinity of moist potato
 526 starch. *Starch/Stärke*, 30, 111–114.

527 Nara, S., & Komiya, T. (1983). Studies on the relationship between water-saturated state
 528 and crystallinity by the diffraction method for moistened potato starch. *Starch/Stärke*,
 529 35, 407–410.

- 530 Otsuka, M., Nishizawa, J., Fukura, N., & Sasaki, T. (2012). Characterization of poly-
531 amorphous indomethacin by terahertz spectroscopy. *Journal of Infrared, Millimeter,*
532 *and Terahertz Waves*, 33, 953–962.
- 533 Park, S., Baker, J. O., Himmel, M. E., Parilla, P. A., & Johnson D. K. (2010). Cellulose
534 crystallinity index: measurement techniques and their impact on interpreting cellulase
535 performance. *Biotechnology for Biofuels*, 3, 1–10.
- 536 Pérez, S., & Bertoft, E. (2010). The molecular structures of starch components and their
537 contribution to the architecture of starch granules: A comprehensive review.
538 *Starch/Stärke*, 62, 389–420.
- 539 Popov, D., Buléon, A., Burghammer, M., Chanzy, H., Montesanti, N., Putaux, J. L., ...
540 Riekkel, C. (2009). Crystal structure of A-amylose: A revisit from synchrotron
541 microdiffraction analysis of single crystals. *Macromolecules*, 42, 1167–1174.
- 542 Pozo, C., Rodríguez-Llamazares, S., Bouza, R., Barral, L., Castaño, J., Müller, N., &
543 Restrepo, I. (2018). Study of the structural order of native starch granules using
544 combined FTIR and XRD Analysis. *Journal of Polymer Research*, 25, 266.
- 545 Sarko, A., & Wu, H. C. H. (1978). The crystal structures of A-, B- and C-polymorphs of
546 amylose and starch. *Starch/Stärke*, 30, 73–78.
- 547 Sevenou, O., Hill, S. E., Farhat, I. A., & Mitchell, J. R. (2002). Organisation of the

external region of the starch granule as determined by infrared spectroscopy.

International Journal of Biological Macromolecules, 31, 79–85.

Strachan, C. J., Rades, T., Newnham, D. A., Gordon, K. C., Pepper, M., & Taday, P. F. (2004). Using terahertz pulsed spectroscopy to study crystallinity of pharmaceutical materials. *Chemical Physics Letters*, 390, 20–24.

Strachan, C. J., Taday, P. F., Newnham, D. A., Gordon, K. C., Zeitler, J. A., Pepper, M., & Rades, T. (2005). Using terahertz pulsed spectroscopy to quantify pharmaceutical polymorphism and crystallinity. *Journal of Pharmaceutical Sciences*, 94, 837–846.

Takeuchi, I., Tomoda, K., Nakajima, T., Terada, H., Kuroda, H., & Makino, K. (2012). Estimation of crystallinity of trehalose dihydrate microspheres by usage of terahertz time-domain spectroscopy. *Journal of Pharmaceutical Sciences*, 101, 3465–3472.

Tang, H. R., Godward, J., & Hills, B. (2000). The distribution of water in native starch granules-a multinuclear NMR study. *Carbohydrate Polymers*, 43, 375–387.

Tonouchi, M. (2007). Cutting-edge terahertz technology. *Nature Photonics*, 1, 97–105.

True, A. B., Schroeck, K., French, T. A., & Schmuttenmaer, C. A. (2011). Terahertz spectroscopy of histidine enantiomers and polymorphs. *Journal of Infrared, Millimeter, and Terahertz Waves*, 32, 691–698.

van Soest, J. J. G., Tournois, H., de Wit, D., & Vliegthart, J. F. G. (1995). Short-range

566 structure in (partially) crystalline potato starch determined with attenuated total
 567 reflectance Fourier-transform IR spectroscopy. *Carbohydrate Research*, 279, 201–
 568 214.

569 van Soest, J. J. G., & Vliegenthart J. F. G. (1997). Crystallinity in starch plastics:
 570 consequence for material properties. *Trends in Biotechnology*, 15, 208–213.

571 Vieira, F. S., & Pasquini, C. (2014). Determination of cellulose crystallinity by terahertz-
 572 time domain spectroscopy. *Analytical Chemistry*, 86, 3780–3786.

573 Walther, M., Fischer, B. M., & Jepsen, P. U. (2003). Noncovalent intermolecular forces
 574 in polycrystalline and amorphous saccharides in the far Infrared. *Chemical Physics*,
 575 288, 261–268.

576 Wang, C., Tang, C. H., Fu, X., Huang, Q., & Zhang, B. (2016). Granular size of potato
 577 starch affects structural properties, octenylsuccinic anhydride modification and
 578 flowability. *Food Chemistry*, 212, 453–459.

579 Warren, F. J., Gidley, M. J., & Flanagan, B. M. (2016). Infrared spectroscopy as a tool to
 580 characterise starch ordered structure - a joint FTIR-ATR, NMR, XRD and DSC Study.
 581 *Carbohydrate Polymers*, 139, 35–42.

582 Xu, J., Ma, Z., Ren, N., Li, X., Liu, L. & Hu, X. (2019). Understanding the multi-scale
 583 structural changes in starch and its physicochemical properties during the processing

584 of chickpea, navy bean, and yellow field pea seeds. *Food Chemistry*, 289, 582–590.

585 Yang, L., Weng, S., Ferraro, J. R., & Wu, J. (2001). Far infrared study of some mono-and

586 disaccharides. *Vibrational Spectroscopy*, 25, 57–62.

587 Yangcheng, H., Jiang, H., Blanco, M., & Jane J. (2013). Characterization of normal and

588 waxy corn starch for bioethanol production. *Journal of Agricultural and Food*

589 *Chemistry*, 61, 379–386.

590 Zhang, B., Dhital, S., & Gidley, M. J. (2013). Synergistic and antagonistic effects of α -

591 amylase and amyloglucosidase on starch digestion. *Biomacromolecules*, 14, 1945–

592 1954.

593 Zhang, B., Wang, K., Hasjim, J., Li, E., Flanagan, B. M., Gidley, M. J. & Dhital, S. (2014).

594 Freeze-drying changes the structure and digestibility of B-polymorphic starches.

595 *Journal of Agricultural and Food Chemistry*, 62, 1482–1491.

596 Zhbakov, R. G, Andrianov, V. M, & Marchewka, M. K. (1997). Fourier transform IR

597 and Raman spectroscopy and structure of carbohydrates. *Journal of Molecular*

598 *Structure*, 436–437, 637–654.

599 Zobel, H. F. (1988). Molecules to granules: A comprehensive starch review. *Starch/Stärke*,

600 40, 44–50.